THE JOURNAL OF BIOLOGICAL CHEMISTRY VOL. 283, NO. 6, pp. 3338–3348, February 8, 2008

Domain Architecture and Biochemical Characterization of Vertebrate Mcm10*[S]

Received for publication, July 30, 2007, and in revised form, December 4, 2007 Published, JBC Papers in Press, December 6, 2007, DOI 10.1074/jbc.M706267200

Patrick D. Robertson[‡1], Eric M. Warren[‡1,2], Haijiang Zhang[‡1], David B. Friedman[§], Jeffrey W. Lary[¶], James L. Cole[¶], Antonin V. Tutter[‖], Johannes C. Walter[‖], Ellen Fanning[‡], and Brandt F. Eichman[‡§3]**

*From the [‡]Department of Biological Sciences, [§]Department of Biochemistry, and **Center for Structural Biology, Vanderbilt University, Nashville, Tennessee 37232, [¶]National Analytical Ultracentrifugation Facility, University of Connecticut, Storrs, Connecticut 06269, and [‖]Department of Biological Chemistry and Molecular Pharmacology, Harvard Medical School, Boston, Massachusetts 02115*

Mcm10 plays a key role in initiation and elongation of eukaryotic chromosomal DNA replication. As a first step to better understand the structure and function of vertebrate Mcm10, we have determined the structural architecture of *Xenopus laevis* Mcm10 (xMcm10) and characterized each domain biochemically. Limited proteolytic digestion of the full-length protein revealed N-terminal-, internal (ID)-, and C-terminal (CTD)-structured domains. Analytical ultracentrifugation revealed that xMcm10 self-associates and that the N-terminal domain forms homodimeric assemblies. DNA binding activity of xMcm10 was mapped to the ID and CTD, each of which binds to single- and double-stranded DNA with low micromolar affinity. The structural integrity of xMcm10-ID and CTD is dependent on the presence of bound zinc, which was experimentally verified by atomic absorption spectroscopy and proteolysis protection assays. The ID and CTD also bind independently to the N-terminal 323 residues of the p180 subunit of DNA polymerase α-primase. We propose that the modularity of the protein architecture, with discrete domains for dimerization and for binding to DNA and DNA polymerase α-primase, provides an effective means for coordinating the biochemical activities of Mcm10 within the replisome.

Eukaryotic DNA replication is carried out by large multiprotein machines that coordinate DNA unwinding and synthesis at the replication fork. Initiation of replication involves ordered assembly of the replisome and local denaturation of duplex DNA at the origin followed by replisome activation. Screens for mutants defective in minichromosome maintenance (Mcm)[4] and DNA replication in yeast identified a number of factors essential for replication (1–4). Pre-replicative complexes composed of the origin recognition complex, Cdc6, Cdt1, and the hexameric Mcm2–7 helicase are assembled in G_1 (for review, see Ref. 5) and converted into active replication forks at the onset of S phase. Mcm10 loads onto chromatin after pre-replicative complex assembly (6, 7) and stimulates phosphorylation of Mcm2–7 by Dbf4-Cdc7 kinase (8). Once Mcm10 is present, Cdc45 and GINS are loaded onto chromatin (6, 9, 10) and form a Cdc45/Mcm2–7/GINS helicase complex (11–14). Cyclin- and Dbf4-dependent kinases together with Sld2, Sld3, and Dpb11 in budding yeast (15, 16) stimulate origin unwinding, which is signified by recruitment of replication protein A to single-stranded DNA (17, 18). Mcm10, Cdc45, and replication protein A facilitate subsequent loading of DNA polymerase α-primase (pol α) onto chromatin (7, 9, 19, 20). The association of proliferating cell nuclear antigen, RFC, and replicative DNA polymerases δ and ϵ with the origin completes the replisome (for review, see Ref. 21).

A number of interactions have been observed between Mcm10 and proteins found in the pre-replicative complexes and at the replication fork. Mcm10 is a component of active replication complexes in *Xenopus* and budding yeast (12, 14) and is associated with chromatin throughout S-phase (7). Mcm10 interacts genetically with Mcm2–7, DNA pol δ and ϵ, origin recognition complex, and Dpb11 (2, 22–24). *In vitro*, interactions of Mcm10 with initiation factor origin recognition complex, Mcm2–7, Cdc45, and Cdc7/Dbf4 have been observed by co-immunoprecipitation from cell extracts (8, 22, 24, 25). Importantly, Cdc45 and replication protein A cannot load onto chromatin in Mcm10-depleted *Xenopus* egg extracts, preventing DNA unwinding (6). Thus, the essential role of Mcm10 in initiation links the pre-replicative complexes with origin unwinding.

Several lines of evidence suggest that Mcm10 migrates with the elongating replication fork through association with DNA polymerases and DNA. *Schizosaccharomyces pombe* Mcm10 (spMcm10) affects chromatin binding and subnuclear distribution of pol α (19, 26), and *Saccharomyces cerevisiae* Mcm10 (scMcm10) has been shown to interact with and stabilize the

* This work was funded by National Institutes of Health Grants GM080570 (to B. F. E.) and GM52948 (to E. F.) and by the Vanderbilt Discovery Grant Program. Additional support for facilities came from the Vanderbilt Center in Molecular Toxicology Grant P30 ES000267. The costs of publication of this article were defrayed in part by the payment of page charges. This article must therefore be hereby marked "*advertisement*" in accordance with 18 U.S.C. Section 1734 solely to indicate this fact.

[S] The on-line version of this article (available at http://www.jbc.org) contains supplemental Figs. S1–S5.

[1] These authors contributed equally to this work.

[2] Supported from the Molecular Biophysics Training Grant T32 GM08320.

[3] To whom correspondence should be addressed: VU Station B, Box 35-1634, Nashville, TN 37235-1634. Fax: 615-343-6707; E-mail: brandt.eichman@vanderbilt.edu.

[4] The abbreviations used are: Mcm, minichromosome maintenance; ssDNA, single-stranded DNA; dsDNA, double-stranded DNA; pol α, DNA polymerase α-primase; MALDI-TOF, matrix-assisted laser desorption/ionization time-of-flight; MS, mass spectrometry; NTD, N-terminal domain; ID, internal domain; CTD, C-terminal domain; FL, full-length; GST, glutathione *S*-transferase; Trx, thioredoxin; GFAA, graphite furnace atomic absorption; MBP, maltose-binding protein; aa, amino acids; GINS, Sld5 (go), Psf1 (ichi), Psf2 (nii), Psf3 (san).

catalytic subunit of pol α *in vivo* (7, 27). *In vitro*, spMcm10 interacts with and stimulates the activity of the catalytic (polymerase) subunit of pol α (28) and has been shown to contain primase activity (29). Additionally, an interaction between diubiquitinated scMcm10 and proliferating cell nuclear antigen is essential for replication in budding yeast (30). Finally, spMcm10 binds to single (ss)- and double-stranded (ds) DNA *in vitro*, and DNA binding activity is localized in the N-terminal 300 residues of the protein (28). The interactions between Mcm10, DNA, and pol α have led to the suggestion that Mcm10 helps to recruit pol α to the replisome and may regulate its activity. Studies in *Xenopus* extracts have demonstrated that when an elongating fork stalls, Mcm10 and DNA polymerases α, δ, and ϵ are uncoupled from the Cdc45/Mcm2–7/GINS helicase (12).

Sequence alignments of Mcm10 from divergent eukaryotes show stretches of consecutive residues that are phylogenetically conserved (Fig. 1*A*), suggesting that these regions may be important to the structure and function of the protein. Mcm10 from Metazoa contains ~100–300 residues not present in the yeast proteins, and conservation from yeast to human is limited to ~200-amino acids in the middle of the protein. Consistent with Mcm10 DNA binding activity, the conserved central region contains an invariant CCCH zinc binding motif (22, 23, 31) and a putative oligonucleotide/oligosaccharide binding fold (27).

The lack of sequence similarity outside of the central region raises a question of whether the function of Mcm10 is conserved from yeast to Metazoa. In the present study we report the first structure-function analysis of vertebrate Mcm10 using the *Xenopus laevis* protein (xMcm10). Limited proteolytic digestion of xMcm10 revealed the protein to be composed of at least three structural domains, an N-terminal domain (NTD) that forms homodimers in solution and highly conserved internal (ID) and C-terminal domains (CTD) that bind to ssDNA, dsDNA, and to the p180 subunit of pol α. Our results confirm and extend previous work from yeast and suggest that vertebrate Mcm10 contains a CTD not present in the yeast orthologs.

EXPERIMENTAL PROCEDURES

Cloning, Expression, and Purification of xMcm10—The cDNAs encoding full-length xMcm10 (FL, 1–860) and deletion fragments 1–145, 1–230, 230–427, 427–860, and 596–860 were PCR-amplified from a previously described plasmid encoding a GST-xMcm10 fusion (6). The FL-xMcm10 PCR product was ligated into a modified pMAL-c2x vector (New England Biolabs) to generate an maltose-binding protein (MBP)-xMcm10-His_6 fusion protein, and xMcm10 fragments were ligated into a modified pET-32a plasmid (Novagen) to generate N-terminal thioredoxin (Trx)-His_6 fusion proteins. Protein was overexpressed in *Escherichia coli* BL21(DE3) cells in Luria-Bertani medium supplemented with 100 μg/ml ampicillin, 5 μM $ZnSO_4$, and 0.5 mM isopropyl 1-thio-β-D-galactopyranoside. Proteins were overexpressed at 22 °C for 4 h (FL) or at 16 °C for 16 h (fragments). The cells were resuspended in 50 mM Tris-HCl, pH 7.5, 500 mM NaCl, 10% glycerol, and lysed under pressure (25,000 p.s.i.) using an EmulsiFlex-C3 homogenizer (Avestin, Inc.). FL-xMcm10 was purified by tandem nickel-nitrilotriacetic acid and amylose affinity chromatography, cleavage of the MBP tag, and SP-Sepharose cation exchange. Protein was concentrated and stored in FL buffer (20 mM Tris-HCl, pH 7.5, 500 mM NaCl, 1 mM dithiothreitol, and 5% glycerol). xMcm10 fragments were purified by nickel-nitrilotriacetic acid affinity chromatography followed by cleavage of the Trx-His_6 tag. The cleaved proteins were further purified by cation exchange (fragments 230–427, 427–860, 596–860) or anion exchange (1–145 and 1–230) chromatography followed by gel filtration on a Superdex^{TM} 200 preparative column (GE Healthcare) that had been equilibrated with S-200 buffer (20 mM Tris-HCl, pH 7.5, 100 mM NaCl, 5% glycerol, 4 mM β-mercaptoethanol. Structural integrity of fragment proteins was verified by circular dichroism spectroscopy.

Limited Proteolysis and Fragment Identification—Proteolysis experiments were carried out in S-200 buffer, in which 5–20 μM xMcm10 was incubated with 1–200 ng of protease (trypsin, α-chymotrypsin, elastase, or endoproteinase-Glu-C) in a 10-μl reaction at 37 °C for 30 min. Proteolysis protection reactions contained 10 mM EDTA. Proteases were inactivated by adding 10 μl of SDS-PAGE sample buffer (63 mM Tris-HCl, pH 6.8, 700 mM β-mercaptoethanol, 2% w/v SDS, 0.03% w/v bromphenol blue, and 10% glycerol) and heating for 5 min at 95 °C. Proteolytic fragments were separated by SDS-PAGE and visualized by Coomassie Blue staining.

Proteolytic fragments from MBP-xMcm10-His_6 were excised from the SDS-PAGE gel and subjected to in-gel digestion with Trypsin Gold (Promega) using standard procedures (32). The resulting peptides were analyzed by matrix-assisted laser desorption/ionization, time-of-flight mass spectrometry (MALDI-TOF MS) and TOF/TOF tandem MS using a Voyager 4700 (Applied Biosciences, Framingham MA). Peptide ion masses (M+H) were accurate to within 20 ppm after internal calibration using either trypsin autolytic peptides or xMcm10-derived peptides confirmed by TOF/TOF MS.

Molecular masses of xMcm10 domains resulting from proteolysis of deletion mutants Δ1, Δ2, and Δ3 were obtained by MALDI-TOF mass spectrometry of the proteolysis reactions before SDS-PAGE. Reactions were concentrated in 0.1% trifluoroacetic acid, mixed with 3 μl of saturated sinapinic acid in 60:40 (v/v) acetonitrile:1% trifluoroacetic acid/distilled H_2O, and 1 μl was deposited onto a gold 100-well plate. Mass spectra were acquired on a Perceptive Biosystems Voyager Elite TOF spectrometer equipped with a laser desorption ionization source and an extended-path ion reflector. Protein standards from Sigma (MSCAL1-1KT) were used for mass calibration. For N-terminal sequencing of xMcm10 domains, intact proteolytic fragment proteins were transferred from SDS gel to a polyvinylidene difluoride membrane, stained with Ponceau S, extracted from the membrane, and subjected to Edman degradation chemistry using an Applied Biosystems Model 492HT Protein/Peptide Sequencer equipped with an on-line phenylthiohydantoin-derivative analyzer.

Zinc Quantitation—Quantitative analysis of zinc bound to xMcm10 was performed using graphite furnace atomic absorption (GFAA) spectroscopy. Analyses were performed using a PerkinElmer Life Sciences HGA SIMAA 6000 graphite furnace equipped with an AAnalyst 800 GFAA/FLAA spectrophotom-

eter. xMcm10 domains were quantified by absorbance spectroscopy at 280 nm using extinction coefficients of 0.092 (NTD), 1.09 (ID), and 0.524 (CTD) ml·mg^{-1}·cm^{-1}.

Gel Filtration Chromatography and Analytical Ultracentrifugation—Size exclusion chromatography of FL-xMcm10 was performed on a Superose 6 column (GE Healthcare) equilibrated with 20 mM Tris-HCl, pH 7.5, 500 mM NaCl, 5% glycerol, and 1 mM dithiothreitol. xMcm10 domains were eluted from an analytical Superdex^{TM} 200 column (GE Healthcare) equilibrated with S-200 buffer. 50-μl solutions of either xMcm10 (~1–2 mg/ml) or molecular weight standards were eluted at 0.5 ml/min. The standard curve was generated from thyroglobulin (670 kDa), aldolase (158 kDa), albumin (67 kDa), chicken ovalbumin (44 kDa), equine myoglobin (17 kDa), and vitamin B_{12} (1.4 kDa).

Sedimentation velocity analysis was conducted at 20 °C and 55,000 rpm using interference optics with a Beckman-Coulter XL-I analytical ultracentrifuge. Double sector synthetic boundary cells equipped with sapphire windows were used to match the sample and reference menisci. FL-xMcm10 was prepared in FL-buffer, and NTD and CTD were prepared in S-200 buffer. The data were initially analyzed using the program DCDT+, which computes the apparent sedimentation coefficient distribution function g(s*) using the time-derivative method (33, 34). For CTD, the molecular weight and sedimentation coefficient of the main component was obtained by global fitting of the data sets collected at multiple concentrations to a hybrid discrete-continuous model with Sedphat (35). For NTD, the data were fit to a monomer-dimer equilibrium model using the programs Sedanal (36) and Sedphat. Molecular masses, partial specific volumes, and solvent densities were calculated using the SEDNTERP program (37).

Fluorescence Anisotropy—DNA binding was measured by following an increase in fluorescence anisotropy as protein (MBP-xMcm10-His_6, NTD, ID, or CTD) was added to oligonucleotide d(TGACTACTACATGGTTGCCTACCAT) containing a 6-carboxyfluorescein moiety at the 3′-end either alone (ssDNA) or annealed to an excess of the complementary strand (dsDNA). Forked DNA substrate tested against full-length Mcm10 was generated from two 50-mer deoxyoligonucleotides in which dC_{25} was added to the 3′-end of the sequence above and to the 5′-end of the complementary sequence. For Mcm10-ID and -CTD, forked and bubble DNA substrates were generated from the sequences d(**GGTAGGCACG**AACCATGTAGTAGTA)/d(AACCATGTAGTAGTA**CGTGCCTACC**) and d(**GGTAGGCACG**AACCATGTAGTAGTA**GGCAATCAGC**)/d(**GCTGATTGC**CAACCATGTAGTAGTA**CGTGCCTACC**), respectively, in which the boldface denotes duplex regions. Protein was added over the concentration range of 0.05–50 μM to a solution containing 25 nM DNA in S-200 buffer. For EDTA titrations, the buffer was supplemented with 0.1, 1, 10, and 25 mM EDTA. Polarized fluorescence intensities using excitation and emission wavelengths of 495 and 515 nm, respectively, were measured for 30 s (1/*s*) and averaged. Anisotropy (*r*) was calculated using the equation $r = (I_{par} - I_{perp})/(I_{par} + 2I_{perp})$, where I_{par} and I_{perp} are the observed fluorescence intensities recorded through polarizers oriented parallel and perpendicular, respectively, to the direction of vertically polarized light. Dissociation constants (K_d) were derived by fitting a simple two-state binding model to data from three experiments using Kaleidagraph 3.6 (Synergy Software).

Mcm10-Pol α Binding Assay—Recombinant DNA polymerase α-primase was purified by immunoaffinity chromatography from extracts of Hi-5 insect cells co-infected with four recombinant baculoviruses as previously described (38). The p180 subunit was prepared identically except only one recombinant baculovirus was used for infection. p180N (aa 1–323) was amplified by PCR on a cDNA template pBR322-p180 and cloned into the BamHI/EcoRI sites of a pGEX-2T expression vector (GE Healthcare). GST fusion proteins were expressed and purified by glutathione-agarose affinity chromatography as described previously (39).

For the binding experiments, a total of 7 μg of purified polymerase α-primase or p180 was incubated with SJK132-20 antibodies covalently coupled to Sepharose-4B beads (GE Healthcare), or 7 μg of purified p180N was incubated with glutathione-agarose beads (Sigma-Aldrich) in binding buffer (30 mM HEPES-KOH, pH 7.8, 10 mM KCl, 7 mM $MgCl_2$) containing 2% nonfat dry milk for 1 h at 4 °C with end-over-end rotation. Reactions contained either 5 or 15 μg of Trx-His_6-xMcm10-domain proteins. The beads were washed once with binding buffer, three times with wash buffer (30 mM HEPES-KOH, pH 7.8, 75 mM KCl, 7 mM $MgCl_2$, 0.25% inositol, 0.1% Nonidet P-40), and once with binding buffer (rotated for 10 min during each wash). The beads were resuspended in 30 μl of 2× SDS-PAGE loading buffer and heated at 100 °C for 5 min. Half of each sample was analyzed by 10% SDS-PAGE and immunoblotting with monoclonal antibody 2CT25, specific for the p180 subunit of polymerase α-primase, rabbit anti-GST (Invitrogen) for p180N, and H-15 anti-His (Santa Cruz Biotechnology) for xMcm10 domains. Trx-only control experiments were performed to confirm that pol α, p180, and p180N did not interact with the Trx affinity tag.

DNA Primase Assay—Oligoribonucleotide synthesis activity was measured as previously described for spMcm10 (29). Briefly, 2–8 pmol of purified xMcm10 or 0.6–2.4 pmol of purified polymerase α-primase were incubated at 37 °C for 40 min with 1.0 μM dT_{50}, 25 μCi of [α-^{32}P]ATP, and 0.1 mM ATP in a 10 μM reaction containing 40 mM Tris-HCl, pH 7.4, 10 mM magnesium acetate, 1 mM dithiothreitol, and 100 μg/ml bovine serum albumin. Reactions were treated with 1 unit of calf intestine phosphatase at 37 °C for 40 min. After the addition of 3 μl of sequencing gel running buffer (98% formamide, 10 mM EDTA, pH 8.0, 0.1% xylene cyanol, 0.1% bromphenol blue), samples were heated to 98 °C for 5 min and separated on a 25% polyacrylamide, 7 M urea gel. RNA was visualized by autoradiography.

RESULTS

xMcm10 Contains Three Structural Domains—In the current study experiments to characterize the domain architecture of vertebrate Mcm10 were carried out using the *X. laevis* ortholog because of previous investigations of the function of the protein using *Xenopus* egg extracts (6, 40). Homology exists in three distinct regions of the protein (Fig. 1*A*, supplemental Fig. S1). The internal region (aa 240–430) is highly conserved

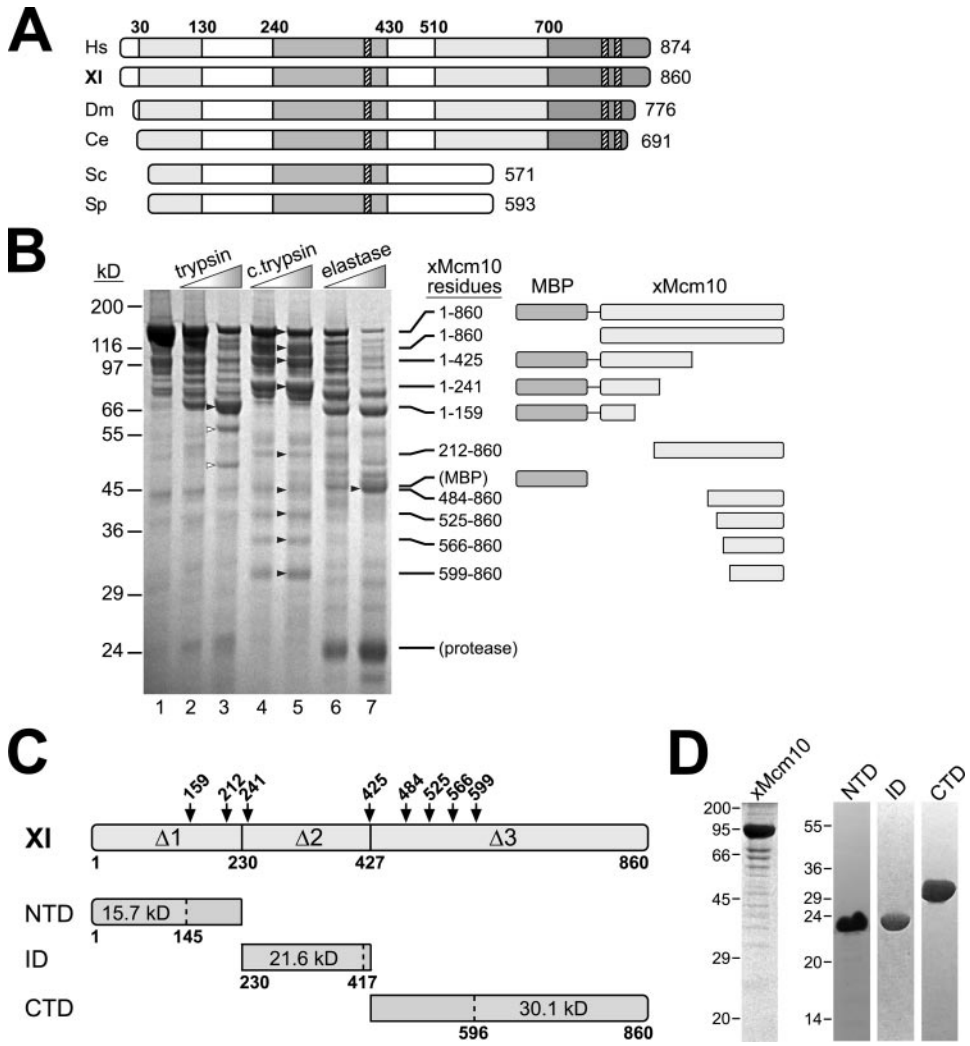

FIGURE 1. **Domain architecture of Mcm10.** *A*, schematic alignment of Mcm10 sequences from *Homo sapiens* (*Hs*), *X. laevis* (*Xl*), *Drosophila melanogaster* (*Dm*), *Caenorhabditis elegans* (*Ce*), *S. cerevisiae* (*Sc*), and *S. pombe* (*Sp*). *Light* and *dark gray bars* indicate moderate and high sequence conservation, respectively, and *hatched boxes* represent invariant cysteine/histidine clusters likely involved in zinc coordination. A full sequence alignment is available as online supplemental data. *B*, limited proteolytic digestion of xMcm10. 50 pmol MBP-xMcm10 (*lane 1*) was subjected to proteolysis by trypsin (25 and 100 ng, *lanes 2* and *3*), chymotrypsin (*c.trypsin*) (100 and 200 ng, *lanes 4–5*), and elastase (10 and 25 ng, *lanes 6* and *7*) and visualized by Coomassie Blue-stained SDS-PAGE. Major proteolytic fragments marked with *black arrowheads* were unambiguously identified by MALDI-TOF and TOF/TOF tandem mass spectrometry and are shown schematically to the *right*. *Bands* marked with *white arrowheads* contained several co-migrating Mcm10 fragments. The full peptide coverage map used to identify fragment endpoints is available as online supplemental data. *C*, three truncation fragments (Δ*1*, Δ*2*, Δ*3*) of xMcm10 were purified and subjected to limited proteolysis to reveal stable domains NTD, ID, and CTD. Proteolytically sensitive sites identified in *panel B* are *highlighted* with *arrows* on *top* of the full-length protein schematic. Molecular masses and N-terminal sequences shown for each proteolytic fragment were identified by mass spectrometry and Edman degradation. *D*, Coomassie-stained SDS-PAGE of purified full-length xMcm10, NTD, ID, and CTD used in this study.

among all known Mcm10 orthologs, with an overall similarity of 21.3% (39.0% for non-yeast Mcm10). Likewise, the C terminus contains a region of high (aa ~700–860) and moderate (aa 510–700) similarity among higher eukaryotes. However, this region is not present in the yeast proteins (23.3% similarity for metazoan as compared with 3.6% for all eukaryotes). Moderate sequence similarity also exists at the N terminus (10% similarity for aa 1–130 in non-yeast sequences). This sequence analysis immediately suggested the presence of at least three domains tethered by disordered linkers. Consistent with this, no secondary structure was predicted in regions 130–230 and 575–624 (supplemental Fig. S1), and region 130–230 was predicted to be largely disordered.

To experimentally determine the domain organization of Mcm10, the full-length protein was overexpressed in *E. coli* with a cleavable N-terminal MBP tag and a C-terminal His_6 tag. The purified MBP-xMcm10-His_6 protein was subjected to limited proteolytic digestion by trypsin, chymotrypsin, and elastase, and the major proteolytic fragments were identified by MALDI-TOF MS and MALDI-TOF/TOF tandem MS (Fig. 1*B*). Peptide masses were mapped to the xMcm10 amino acid sequence to define domains (supplemental Fig. S2). In most cases the end point regions were defined by peptide ions that were present in the full-length protein but absent in the fragment under study, and in some cases the end point was confirmed with tandem MS on unique peptide(s) that were generated by chymotrypsin cleavage on one side (from limited proteolysis) and trypsin cleavage on the other (from in-gel digestion). Peptides analyzed in this way revealed proteolytic-resistant domains separated by cleavage sites at amino acids 159, 241, 425, 484, 525, 566, and 599 (Fig. 1*B* and supplemental Fig. S2).

Using the proteolytically sensitive regions as a guide, three deletion constructs encompassing the entire protein were designed to define the domain boundaries more accurately: $xMcm10^{1-230}$ (Δ1), $xMcm10^{230-427}$ (Δ2), and $xMcm10^{427-860}$ (Δ3). Each of these proteins were expressed in bacteria, purified, and subjected to limited proteolysis by trypsin (supplemental Fig. S3). Precise endpoints of tryptic fragments were identified by Edman degradation and MALDI mass spectrometry (Fig. 1*C*). Chymotrypsin, elastase, and endoproteinase-Glu-C digestion was also performed (data not shown). Despite the unique specificities of each protease tested, the resulting cleavage patterns were similar for each Mcm10 deletion mutant. Proteolysis of each deletion mutant revealed the presence of smaller fragments that were resistant to digestion and that were consistent with the cleavage pattern of the full-length protein (Fig. 1*B*) and with regions of sequence conservation (Fig. 1*A*). Cleavage of the C-terminal ends of Δ1 and Δ2 yielded $xMcm10^{1-145}$ and

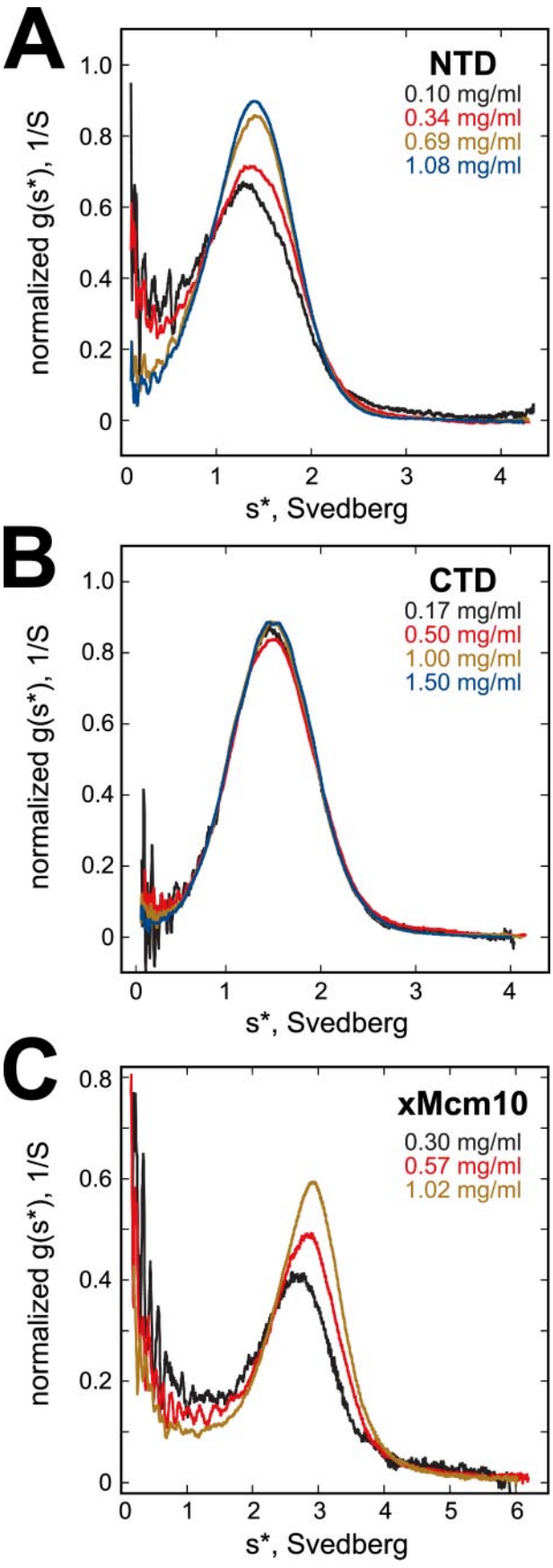

FIGURE 2. **Self-association of xMcm10.** Shown are overlays of normalized g(s*) plots from sedimentation velocity experiments at different concentrations of xMcm10-NTD (*A*), CTD (*B*), and full-length enzyme (*C*). NTD and CTD were prepared in 20 mM Tris, pH 7.5, 100 mM NaCl, 3.5 mM β-mercaptoethanol, and 5% glycerol, and full-length enzyme was prepared in 20 mM Tris, pH 7.5, 500 mM NaCl, 1 mM dithiothreitol, 5% glycerol. Conditions: rotor speed, 55,000 rpm; temperature, 20 °C; interference optics.

xMcm10$^{230-417}$, respectively. For Δ3, ~170 residues were cleaved from the N terminus, yielding xMcm10$^{596-860}$. The resistance of xMcm10$^{1-145}$, xMcm10$^{230-417}$, and xMcm10$^{596-860}$ to further degradation indicates the presence of stable tertiary folds that sterically preclude protease access to their cleavage sites. To prepare for further characterization, regions 1–145 (NTD), 230–417 (ID), and 596–860 (CTD) were subcloned, overexpressed, and purified (Fig. 1*D*). The anomalous electrophoretic mobility of the NTD can be rationalized on the basis of the predicted pI (4.2) and elongated shape of the protein (see below). The NTD, ID, and CTD were relatively stable to further proteolytic digestion, and circular dichroism spectra confirmed the presence of secondary structure in each domain (data not shown).

Dimerization of xMcm10-NTD—Purified scMcm10 and spMcm10 have been reported to oligomerize in solution (8, 29, 31), and human Mcm10 was recently reported to form hexameric assemblies (41). Before a rigorous analysis of xMcm10 oligomerization, we first investigated the hydrodynamic properties of the full-length, NTD, ID, and CTD proteins by gel filtration chromatography (supplemental Fig. S4). The elution volumes of full-length and NTD proteins were considerably less than expected for globular, monomeric proteins. Similarly, the CTD showed a modest decrease in retention volume as compared with that of a 30-kDa protein standard. The elution profile of the ID, on the other hand, corresponded exactly to that of a 22-kDa protein, indicating that this domain does not self-associate. These results raised the question of whether xMcm10 oligomerizes in solution or whether the shape of the protein significantly deviates from a globular fold.

The oligomeric states of the NTD, CTD, and full-length proteins were determined using sedimentation velocity experiments (Fig. 2). Fig. 2*A* shows an overlay of the normalized g(s*) sedimentation coefficient distributions for four concentrations of the NTD. The distributions shift to the right with increasing concentration, indicating reversible self-association. The best fit to the data were obtained using a monomer-dimer equilibrium model. The sedimentation coefficient for the monomer could not be accurately determined due to the fact that the protein is predominantly dimeric over the concentration range tested. Thus, the sedimentation coefficient ratio s(dimer)/s(monomer) was fixed at 1.45, which is the value predicted for a monomer-dimer system (42). The best fit parameters are $s_{20,w}$ (monomer) = 1.22 S, $s_{20,w}$ (dimer) = 1.77 S, a dissociation constant of K_d = 3.1 μM, and a root mean square error of 0.0048 mg/ml. The corrected sedimentation coefficients of the monomer and dimer can be used to calculate frictional ratios, f/f_0, of 1.8 and 2.0, respectively, indicating that the NTD is highly asymmetric.

The normalized g(s*) profiles for the CTD superimpose over the concentration range tested (0.17–1.5 mg/ml), indicating that the system does not undergo reversible association under these conditions. The molecular weight obtained from a global fit of the data to a single species model is 31.0 kDa, which agrees closely with the predicted monomeric value of 30.1 kDa. The frictional

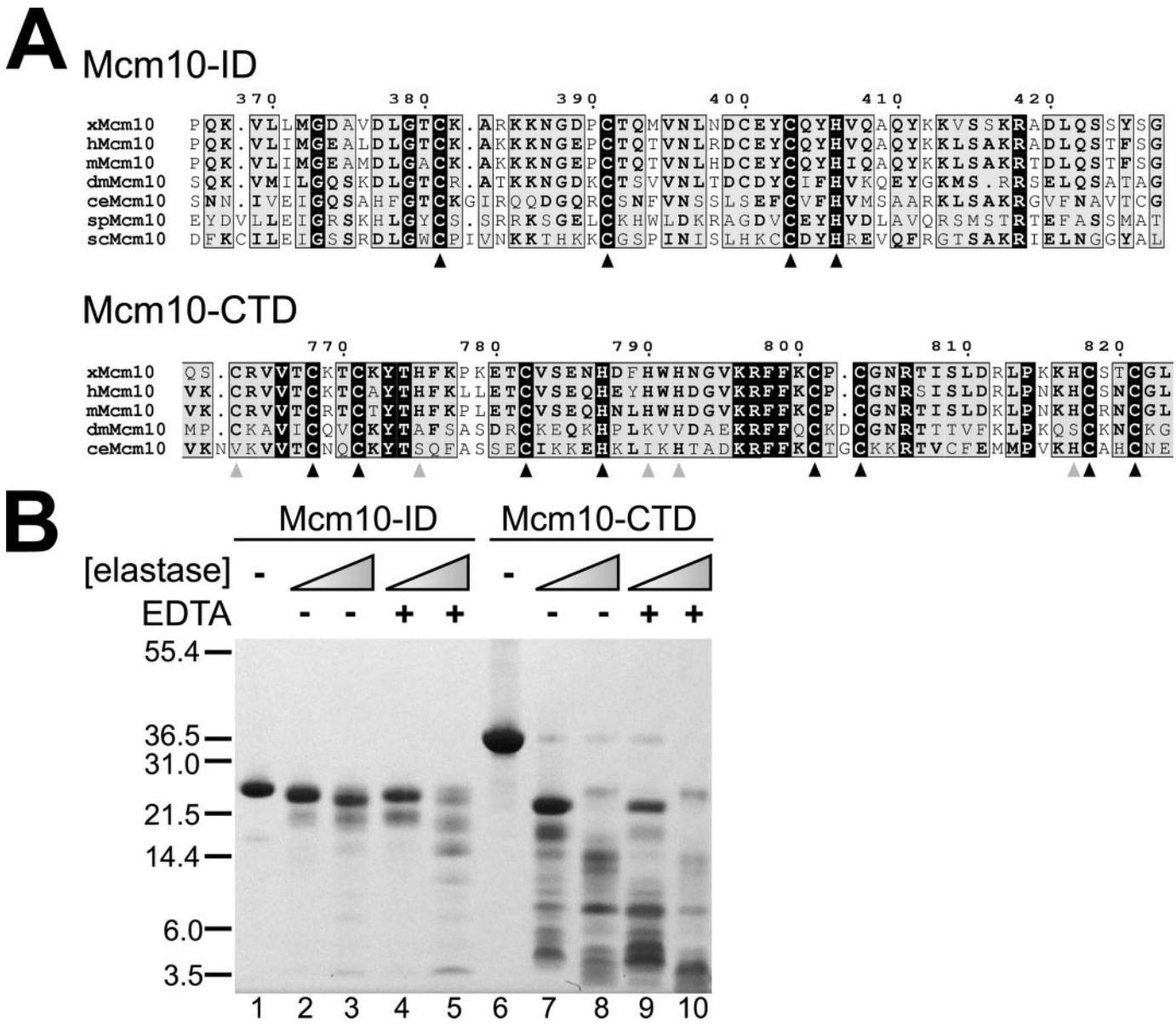

FIGURE 3. **Effect of EDTA on the stability of xMcm10-ID and -CTD.** *A*, sequence alignment of ID and CTD regions containing invariant (*black triangles*) and conserved (*gray triangles*) cysteine and histidine residues likely involved in Zn^{2+} coordination. *B*, SDS-PAGE of elastase-catalyzed proteolysis of ID (*lanes 1–5*) and CTD (*lanes 6–10*) in the presence (*lanes 4*, *5*, *9*, and *10*) and absence (*lanes 2*, *3*, *7*, *8*) of 10 mM EDTA. 100 pmol of each Mcm10 domain was incubated with 10 ng (*lanes 2*, *4*, *7*, and *9*) and 100 ng (*lanes 3*, *5*, *8*, and *10*) elastase.

ratio (f/f_0) of 1.89 indicates that CTD is also quite asymmetric, consistent with its gel filtration behavior.

Fig. 2*C* shows the normalized g(s*) distributions for the full-length enzyme. Like NTD, the distributions shift to the right with increasing concentration, indicating mass-action association. In this case, the presence of lower- and higher-S contaminants precludes further analysis of these data. However, the limiting sedimentation coefficient of ~2.6 S at low concentration indicates that xMcm10 is predominantly monomeric at low concentrations with $f/f_0 \sim 2.2$. Assuming an alternative model where the $s = 2.6$ S species is a dimer yields an unreasonably high $f/f_0 \sim 3.5$.

Zinc-dependent Stability of xMcm10-ID and CTD—Sequence alignments show clusters of highly invariant cysteine and histidine residues in both the ID and CTD (Fig. 3*A*), suggesting that these domains contain zinc binding motifs. Strong evidence has been provided for the presence of a zinc motif in scMcm10 internal region (31), although zinc binding by the CTD has not yet been reported. To verify the presence and determine the stoichiometry of Zn^{2+} in xMcm10 domains, we analyzed each of the domains by GFAA spectroscopy. Molar ratios of Zn^{2+}/xMcm10 for the NTD, ID, and CTD were deter-

TABLE 1
Molar equivalents of Zn^{2+} in xMcm10 domains
Zn^{2+} concentration determined by atomic absorption spectroscopy. TAG, 3-methyladenine DNA glycosylase I.

Protein	Zn^{2+}/xMcm10
xMcm10-NTD	0.16
xMcm10-ID	1.3 ± 0.3
xMcm10-CTD	1.8 ± 0.5
TAG (control)[a]	0.98

[a] Refs. 43 and 44.

mined to be 0.16, 1.3 ± 0.3, and 1.8 ± 0.5, respectively (Table 1). As a positive control, 3-methyladenine DNA glycosylase I (TAG), which has been shown previously to contain 1 Zn^{2+}/molecule (43, 44), was analyzed by GFAA and returned a value of 0.98 Zn^{2+}/TAG. We, therefore, conclude that the NTD, CTD, and ID contain 0, 1, and 2 Zn^{2+} ions, respectively. In support of the GFAA data, x-ray fluorescence emission spectra of xMcm10-ID single crystals, which were grown in the absence of Zn^{2+} in the crystallization buffer, revealed a strong peak at 9.6 keV corresponding to the Zn^{2+} absorption edge (data not shown).

The importance of bound zinc on the tertiary folding of the ID and CTD was investigated by limited proteolysis protection assays. The ID and CTD were subjected to proteolysis by elastase in the presence and absence of EDTA, a known Zn^{2+} chelator. Both domains were more readily degraded in the presence of EDTA (Fig. 3*B*), suggesting that in the absence of bound Zn^{2+}, the ID and CTD were at least partially unfolded and, thus, more susceptible to protease cleavage. Similarly, when the ID and CTD were incubated at room temperature for 10 days in the presence or absence of EDTA, spontaneous degradation was increased in the presence of EDTA (supplemental Fig. S5). These results suggest that the zinc motifs in xMcm10-ID and -CTD play a key role in maintaining the overall structural integrity of these domains.

xMcm10-ID and CTD Are DNA Binding Domains—To quantitatively characterize the DNA binding activity of purified xMcm10, the change in fluorescence anisotropy was monitored as the protein was added to a fluorescein-labeled 25-mer oligonucleotide (Fig. 4). Binding isotherms for MBP-xMcm10-His_6 show that the full-length *Xenopus* protein bound to both ssDNA and dsDNA with the same affinity ($K_d \sim 0.1$ μM) (Fig. 4*A*, Table 2). To determine whether Mcm10 might bind to the replication fork at the ss/dsDNA junction, a forked substrate containing both ssDNA and dsDNA regions was also tested and did not show a difference in binding affinity ($K_d = 0.08 \pm 0.06$ μM) compared with ssDNA and dsDNA (Table 2). Interestingly, in the presence of EDTA, binding of xMcm10 to dsDNA was abolished, whereas the affinity for ssDNA remained unchanged (Fig. 4*A*, Table 2). The overall anisotropy change for ssDNA binding was different between EDTA and non-EDTA titrations, indicating that a change in the tumbling rate of the complex occurred, likely as a result of EDTA-induced local unfolding of the zinc motifs (Fig. 3). These results establish that zinc-dependent structural integrity of xMcm10 is important for the dsDNA binding activity.

Binding of DNA to the NTD, ID, and CTD was then measured to determine the DNA binding domain of xMcm10. No anisotropy change was observed in the presence of the NTD, indicating that this domain does not interact with DNA (Fig. 4*B*). Unexpectedly, both the ID and CTD showed robust binding to both ssDNA and dsDNA (Fig. 4*B*). The affinity of each domain for DNA was roughly the same and was an order of magnitude less than that of the full-length protein (Table 2). Unlike full-length xMcm10, the affinity of each domain for ssDNA was ~2-fold greater than for dsDNA. To test the effect of the Zn^{2+} motifs, binding experiments for each domain were again carried out in the presence of EDTA (Fig. 4*C*). Both

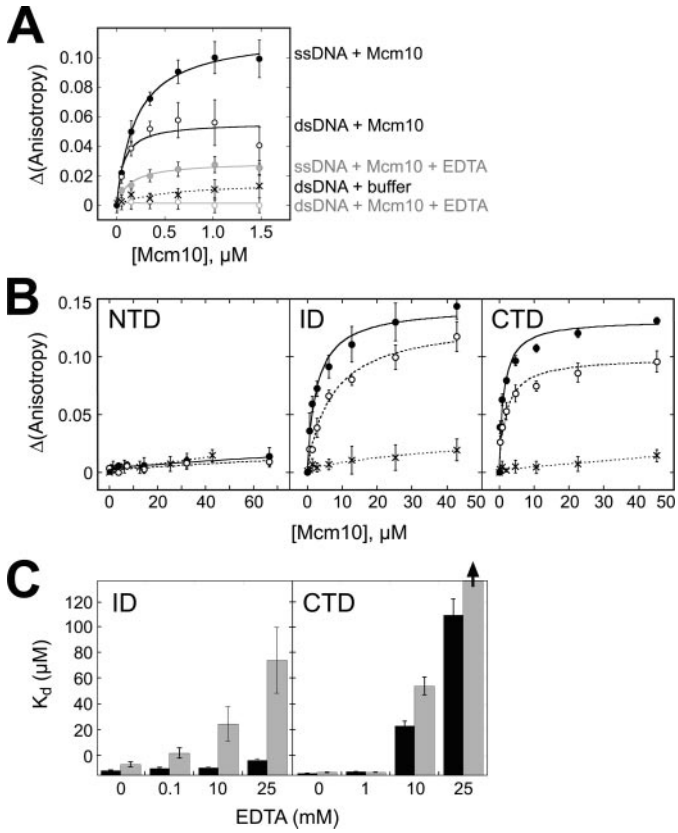

FIGURE 4. **DNA binding of xMcm10.** Binding was monitored as a change in fluorescence anisotropy as full-length (*A*) and isolated domain (*B* and *C*) proteins were titrated into a solution containing fluorescently labeled DNA. *Error bars* represent the S.D. from the average values from three independent measurements. *A*, binding isotherms for full-length MBP-xMcm10-His_6 binding to ssDNA (*filled symbols*) and dsDNA (*open symbols*) in the absence (*black*) and presence (*gray*) of EDTA. A control in which buffer without protein was added to the DNA is shown as *black Xs*. *B*, binding curves for each xMcm10 domain against ssDNA (*closed circles*) and dsDNA (*open circles*), and for buffer-only controls (*Xs*). *C*, the dissociation constants (K_d) for xMcm10-ID and -CTD binding to ssDNA (*black bars*) and dsDNA (*gray bars*) derived from the anisotropy data are plotted as a function of EDTA concentration. The K_d for xMcm10-ID/dsDNA binding in 25 mM EDTA is ≥300 μM, the limit of detection for this assay.

TABLE 2
Dissociation constants for DNA binding

K_d (μM) for xMcm10 binding to deoxyoligonucleotides determined using fluorescence anisotropy. ND, not determined.

	ssDNA[a]	dsDNA[a]	Fork[b]	Bubble[c]
xMcm10[d]	0.12 ± 0.02	0.09 ± 0.03	0.08 ± 0.06	ND
xMcm10[d] + 10 mM EDTA	0.14 ± 0.04	≥300	ND	ND
xMcm10-NTD	≥300	≥300	ND	ND
xMcm10-ID	3.39 ± 0.49	7.83 ± 1.44	3.09 ± 0.99	5.21 ± 1.86
xMcm10-CTD	1.41 ± 0.24	2.21 ± 0.20	2.67 ± 0.34	4.77 ± 2.57

[a] 25-mer ssDNA and dsDNA substrates.
[b] Forked DNA = $(dsDNA)_{25} - 2x(ssDNA)_{25}$ for full-length and $(dsDNA)_{10} - 2x(ssDNA)_{15}$ for domains.
[c] Bubble DNA = $(dsDNA)_{10} - 2x(ssDNA)_{15} - (dsDNA)_{10}$.
[d] Binding data for full-length xMcm10 were measured using MBP-xMcm10-His_6.

xMcm10-ID and -CTD exhibited a dramatic decrease in dsDNA binding affinity as a function of increasing EDTA concentration, whereas the ssDNA affinity was only moderately affected under the same conditions (Fig. 4*C*). Interestingly, EDTA had a greater affect on ssDNA binding to the CTD than the ID, suggesting that ssDNA is able to bind to the ID in the absence of a folded zinc motif.

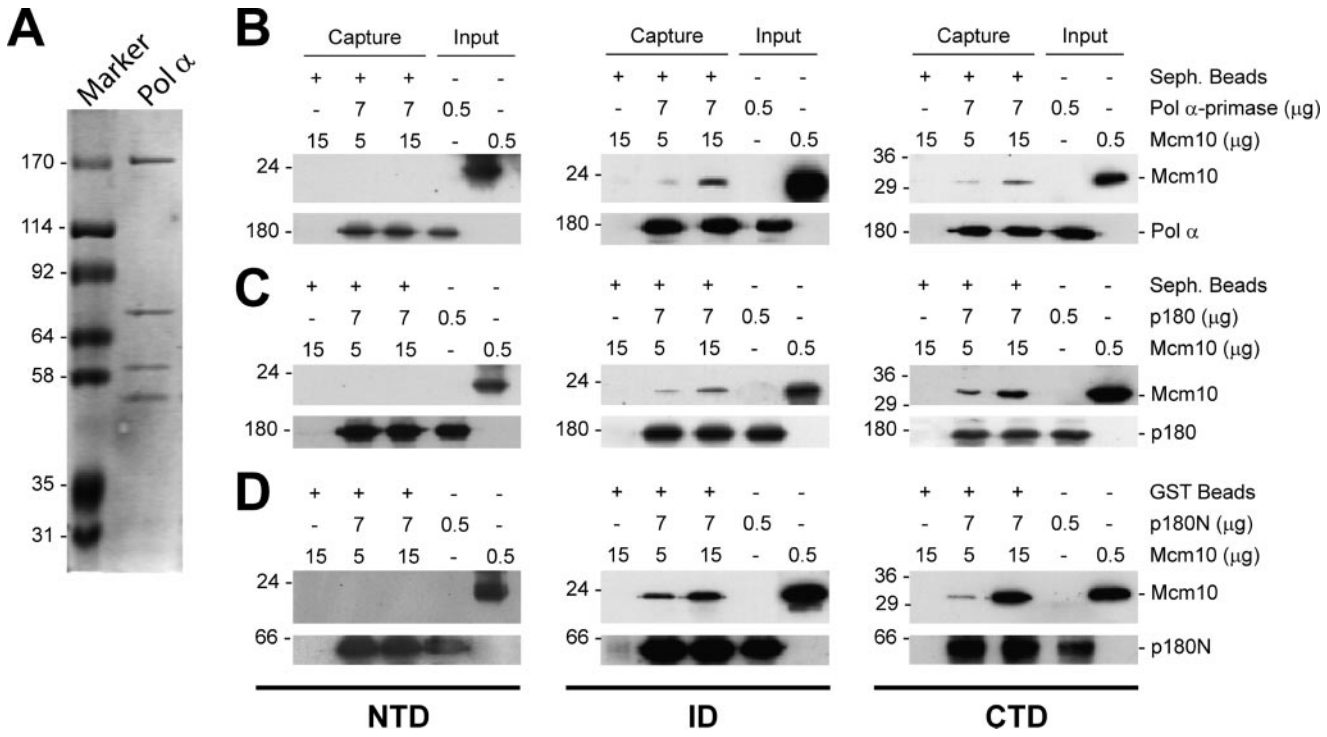

FIGURE 5. **Binding of xMcm10 to the p180 subunit of DNA pol α.** *A*, Coomassie Blue-stained SDS-PAGE gel of purified pol α. *B–D*, affinity capture experiments between xMcm10-NTD (*left panels*), -ID (*center panels*), or -CTD (*right panels*) and pol α (*B*), p180 (*C*), or p180N (*D*). Amounts of protein added to each binding reaction are shown above the Western blots. *B*, the intact pol α complex was mixed with xMcm10 domains NTD, ID, or CTD as indicated and immunoprecipitated on Sepharose beads coupled to SJK132–20 antibodies against the p180 subunit as indicated. Bound xMcm10 domains were detected by Western blotting with an α-His antibody. *C*, the purified catalytic p180 subunit of pol α was mixed with xMcm10 domains and immunoprecipitated as in *B*. Bound xMcm10 domains were detected by Western blotting with an α-His antibody. *D*, GST fused to the N-terminal 323 residues of p180 (*p180N*) was adsorbed on glutathione beads and mixed with xMcm10 domains as indicated. Bound xMcm10 was detected by Western blotting with an α-His antibody.

xMcm10 Binding to DNA Polymerase α-Primase Is Localized to the ID and CTD—We investigated whether vertebrate Mcm10 can undergo direct, physical interactions with pol α, and if so, these interactions can be mapped with the xMcm10 domains. Because purified recombinant human pol α has been shown to substitute functionally for the *X. laevis* protein in *in vitro Xenopus* replication assays (45), human pol α was chosen for these experiments (Fig. 5*A*). The first experiment examined the ability of the purified four-subunit human pol α-primase complex immobilized on beads to capture His-tagged xMcm10 domains from solution. After incubation with purified xMcm10-NTD, ID, or CTD and extensive washing, xMcm10 domains remaining bound to the beads were detected by denaturing gel electrophoresis and anti-His Western blot. Fig. 5*B* shows the results of the pol α-Mcm10 affinity capture, in which both the ID and CTD, but not the NTD, bound to the polymerase complex. The experiment was repeated using only the purified catalytic pol α-p180 subunit in the absence of p48, p58, and p68. Again the NTD was not detected in the bound fraction, and both the ID and CTD bound to p180 (Fig. 5*C*). This result demonstrates that the p180 subunit is sufficient to bind xMcm10-ID and CTD.

We next sought to map the specific Mcm10-binding region of p180. The p180 subunit has a modular organization with an ~300-residue N-terminal region dispensable for polymerase activity, an extended core region containing the conserved polymerase motifs, and a C-terminal region that complexes with the other subunits (46). Only the N-terminal region of p180 binds to SV40 T antigen, an interaction essential for viral DNA replication (47). Based on this information, an N-terminal construct encompassing p180 residues 1–323 (p180N) was tested. GST-tagged p180N immobilized on glutathione-Sepharose was able to capture both the ID and CTD, but not the NTD, consistent with the pol α-primase and p180 pulldown assays (Fig. 5*D*). Thus, p180N is sufficient for Mcm10 interaction. These results also show that as for binding DNA, the ID and CTD function in a coordinated manner.

xMcm10 Does Not Contain Primase Activity—Based on the recent report that spMcm10 contains primase activity (29), we examined the ability of full-length xMcm10 to synthesize an oligoribonucleotide in the presence of a DNA template. Purified xMcm10 that contained no MBP tag (Fig. 1*D*) was incubated with dT_{50} template and [α-^{32}P]ATP, and product RNA was visualized by denaturing PAGE. No radiolabeled products were apparent when compared with a no-enzyme control reaction (Fig. 6). Under identical conditions, pol α-primase showed robust, concentration-dependent formation of oligoribonucleotides ~12 nucleotides in length. This result indicates that a purified preparation of xMcm10 is not capable of priming DNA.

DISCUSSION

Modular Architecture of Mcm10—The present work provides new insight into the role of Mcm10 in initiation and elongation complexes by carrying out the first structure-function analysis of the protein. We have determined using limited

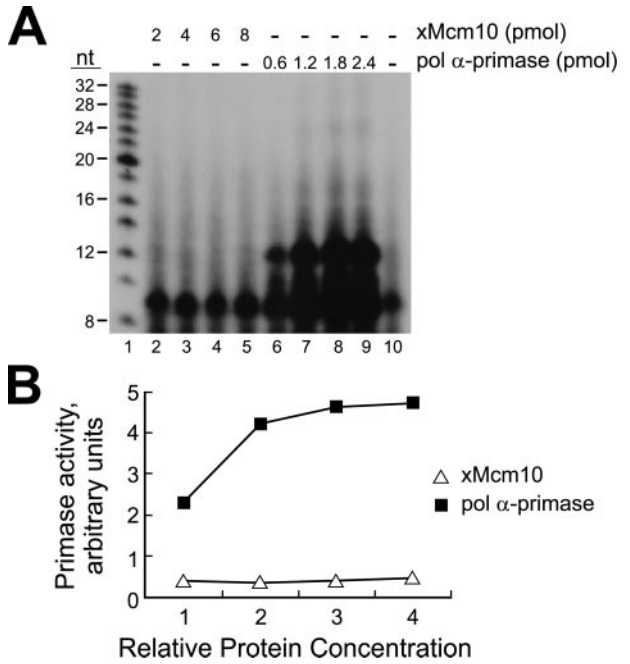

FIGURE 6. **xMcm10 does not contain primase activity.** *A*, oligoribonucleotide synthesis was assayed in reaction mixtures containing dT_{50} template, [α-^{32}P]ATP, and increasing amounts of xMcm10 (*lanes 2–5*) or pol α-primase (*lanes 6–9*). *Lane 10*, negative control lacking xMcm10 and pol α-primase. Radiolabeled products were analyzed by electrophoresis on a 25% denaturing polyacrylamide gel containing 7 M urea. *nt*, nucleotides. *B*, quantitation of the autoradiogram shown in *A*. Primase activity is expressed in arbitrary units, with the reaction containing no protein set to zero. Relative protein concentration corresponds to 0.2, 0.4, 0.6, and 0.8 μM xMcm10 and 0.06, 0.12, 0.18, and 0.24 μM pol α-primase.

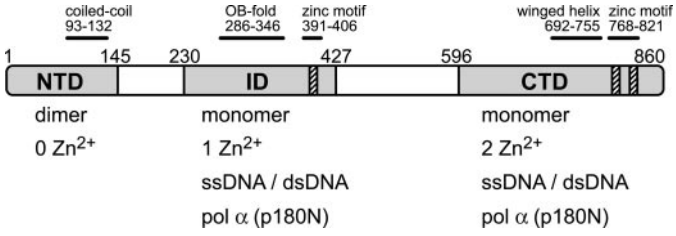

FIGURE 7. **Vertebrate Mcm10.** The schematic summarizes the domain organization and functional regions of xMcm10 identified in this study. The NTD, ID, and CTD are *shaded gray*, and conserved cysteine/histidine clusters predicted to chelate Zn^{2+} are shown as *cross-hatched strips*. Predicted structural motifs are shown as *black bars above the protein*. Listed below each domain are the oligomerization states, number of zinc ions bound, and binding partners.

proteolysis that purified preparations of xMcm10 contain at least three structural domains located from residues 1–145 (NTD), 230–417 (ID), and 596–860 (CTD) (Fig. 7). The extreme proteolytic sensitivity of regions 146–230 and 418–596 suggests that these are exposed flexible linkers connecting each independently folded globular domain. It is likely that these flexible regions become more structured or protected from proteolytic cleavage when Mcm10 is part of the larger multiprotein replisome assembly. Nevertheless, the present work suggests that Mcm10 is at least able to adopt multiple conformations in which each globular domain can move relative to the other two. Such a flexible protein architecture would be necessary for the multiple protein and DNA transactions at an inherently dynamic replication fork. Indeed, many replication proteins have evolved modular architectures with distinct domains that are able to act independently or cooperatively to perform a common task (for review, see Refs. 48 and 49). For example, separate structural domains often provide multiple binding sites that increase the affinity for one ligand or that enable the protein to contact multiple ligands in a concerted or sequential fashion (50).

Structural Features of Mcm10-ID and -CTD—Motifs predicted within the ID and CTD provide a rationale for their interactions with DNA and pol α (Fig. 7). The protein structure prediction Protein Homology/analogY Recognition Engine (PHYRE) program (51) and manual inspection of the xMcm10-CTD primary sequence identified two putative Zn^{2+} binding motifs (aa 692–755 and 768–821) and a three-helical bundle from the winged helix superfamily (aa 692–755) (supplemental Fig. S1). These motifs were not identified in yeast Mcm10 proteins. Previously identified motifs in the conserved ID were also found by this method, including an oligonucleotide/oligosaccharide binding fold (aa 286–346) and zinc motif (391–406) (22, 23, 27). Consistent with the ability of the ID and CTD to bind both DNA and pol α, oligonucleotide/oligosaccharide binding folds, winged helix bundles, and zinc motifs have each been shown to mediate protein-protein interactions in addition to their role in nucleic acid recognition (52–54).

The zinc binding motifs are essential to the structure and function of Mcm10. Mutations in the putative CCCH-type zinc finger within the conserved ID have been shown to disrupt the association of scMcm10 with chromatin (22), to cause growth defects in yeast, and to disrupt the NMR chemical shift dispersion of purified scMcm10 (31). Our atomic absorption data show conclusively that 1 molar eq of zinc is present in the ID and reveal two additional zinc atoms bound to the CTD (Table 1). The effect of Zn^{2+} chelation on Mcm10 DNA binding activity and protein stability (Figs. 3*B* and 4, *A* and *C*; Table 2) helps to explain the dissociation of Mcm10 from chromatin in the *S. cerevisiae mcm10-43* (C320Y in the ID) mutant (4, 22).

The arrangement of the invariant Cys/His clusters in the xMcm10-CTD into a $\mathbf{C}X_2\mathbf{C}X_{10}\mathbf{C}X_4\mathbf{H}X_{13}\mathbf{C}X\mathbf{C}X_{14}\mathbf{C}X_2\mathbf{C}$ consensus sequence (Fig. 3*A*) raises several possibilities for the precise role of the CTD zinc motifs. On one hand, the sequences of each CCCH or CCCC cluster do not deviate significantly from the classical DNA sequence-specific $\mathbf{C}X_2\mathbf{C}X_{12}\mathbf{H}X_3\mathbf{H}$ zinc finger (55). However, there was no difference in binding affinities between either the ID or CTD tested against three different oligonucleotide sequences (data not shown), suggesting that Mcm10 does not recognize DNA in a sequence-specific manner. On the other hand, the two tandem cysteine-rich clusters in the CTD are remarkably similar in sequence to LIM domains and RING finger motifs, which provide protein-binding interfaces important for a variety of cellular functions (for review, see Ref. 56 and 57). It is noteworthy that the CTD zinc motif is immediately adjacent in the primary sequence to a putative winged helical bundle, which was predicted based on its similarity to that of the SCF ubiquitin ligase (58). The globular assembly formed from the RING protein Rbx1, and the winged helical of Cul1 in the SCF complex is an interaction integral to the cullin-RING ubiquitin ligase machinery (59, 60). Thus, the zinc motif in xMcm10-CTD might stabilize the protein fold through a winged helical-RING interaction.

Structural and Functional Differences between Vertebrate and Yeast Mcm10—The lack of sequence conservation within the C-terminal region helps to reconcile differences in DNA binding activities of spMcm10 and xMcm10. The DNA binding affinity for spMcm10 N-terminal (1–303) and C-terminal (295–593) fragments, which are truncated between the putative oligonucleotide/oligosaccharide binding fold and zinc finger of the ID, was the same as that of the full-length protein (28). Full-length xMcm10, on the other hand, bound to DNA with 10-fold greater affinity than xMcm10-ID or -CTD alone (Table 2). Additionally, spMcm10 exhibited a 20-fold preference for ssDNA over dsDNA (28), whereas xMcm10 bound to ssDNA and dsDNA with the same affinity. Although the domain structure of yeast Mcm10 is unknown, these results are consistent with a second DNA binding domain in vertebrate xMcm10-CTD that is not present in the yeast proteins.

The sequence divergence and different DNA binding activities between vertebrate and yeast Mcm10 suggest that these proteins have evolved subtly different functions. An additional DNA binding domain may have evolved in response to the greater complexity of the genome and the lack of specific nucleotide sequences at origins of replication. Alternatively, the additional DNA and pol α binding domain and the lack of detectable primase activity in xMcm10 suggest that vertebrate Mcm10 evolved a means to recruit pol α-primase in lieu of itself priming DNA. Structural studies will be required to determine whether the ID and CTD are classical DNA binding domains, or if they form versatile structural scaffolds commonly observed in replication proteins (46, 61–63).

Perspectives on the Mcm10 Role at the Replication Fork—Structural arrangement of Mcm10 domains together with their macromolecular interactions provides insight into Mcm10 function. Our results are consistent with the notion that Mcm10 recruits pol α to origins of replication (7, 27, 28). With each of two separate domains encompassing DNA and pol α binding activities, Mcm10 might mediate a hand-off mechanism between pol α and DNA. Domain rearrangement to facilitate a handoff between replication proteins and DNA has been proposed for SV40 T antigen-mediated replication protein A loading onto DNA (64).

Evidence is provided here for NTD-mediated dimerization of vertebrate Mcm10 (Fig. 2). Analytical ultracentrifugation clearly showed dimerization of the NTD with a K_d of ~3.1 μM. The full-length enzyme is predominantly monomeric at low concentration but also self-associates, and by analogy to NTD it is likely also a monomer-dimer system. We observed that the NTD of mammalian and yeast Mcm10 contains a predicted coiled-coil (supplemental Fig. S1), a highly asymmetric motif that would explain protein dimerization and the anomalously short gel filtration retention times of Mcm10 constructs containing the NTD. Indeed, frictional ratios calculated from the sedimentation data are indicative of a highly asymmetric protein. These data are consistent with glycerol gradient sedimentation results showing spMcm10 dimerization and suggesting an elongated scMcm10 structure (8) and are intriguing in light of the recent report that human Mcm10 forms a globular homohexameric assembly (41).

NTD-mediated dimerization raises the interesting possibility that Mcm10 interacts with both leading and lagging strand polymerases at a replication fork. Direct physical interactions between Mcm10 and pol α have now been observed in scMcm10, spMcm10, and xMcm10 (27, 28), and genetic studies raise the possibility that Mcm10 also interacts with replicative polymerases δ and ϵ. The coiled-coil interaction would orient both subunits of the Mcm10 dimer in the same direction and consequently provide the polarity needed for the individual subunits to associate with co-directional leading and lagging strands.

The fact that xMcm10 did not preferentially bind to forked DNA substrates (Table 2) suggests that Mcm10 does not reside directly at the fork but, rather, some distance behind the unwinding DNA. On the other hand, interactions between Mcm10 and Mcm2–7 subunits have been observed by yeast two-hybrid (23). Our data suggest that Mcm10 travels with pol α by association with the N-terminal end of p180. This region is dispensable for polymerase activity of p180 (46), suggesting that Mcm10 is capable of interacting with pol α during DNA synthesis. The p68 subunit of pol α has been reported to interact with SV40 T antigen, tethering pol α to the viral replication fork (65, 66), but p68 did not interact with xMcm10 (data not shown). In addition, we were unable to detect a direct interaction between xCdc45 and pol α or between xMcm10 and xCdc45 (data not shown). In summary, the structural studies begun here provide a framework for future studies to elucidate the spatial arrangement of vertebrate Mcm10 and its binding partners and to develop a model for the action of these proteins within the replisome.

Acknowledgments—We thank Tim Bowles, Jami O'Quin, and Laura Mizoue for technical assistance, Hassane McHaourab, Albert Beth, and Charles Cobb for access to fluorometers, and Walter Chazin for critical reading of the manuscript. We thank the Vanderbilt Academic Venture Capital Fund for support of the Proteomics Laboratory. Peptide sequencing was provided by the Protein Analysis Laboratory at Wake Forest University, and atomic zinc analysis was performed by Galbraith Laboratories.

REFERENCES

1. Maine, G. T., Sinha, P., and Tye, B. K. (1984) *Genetics* **106,** 365–385
2. Merchant, A. M., Kawasaki, Y., Chen, Y., Lei, M., and Tye, B. K. (1997) *Mol. Cell. Biol.* **17,** 3261–3271
3. Nasmyth, K., and Nurse, P. (1981) *Mol. Gen. Genet.* **182,** 119–124
4. Solomon, N. A., Wright, M. B., Chang, S., Buckley, A. M., Dumas, L. B., and Gaber, R. F. (1992) *Yeast* **8,** 273–289
5. Blow, J. J., and Dutta, A. (2005) *Nat. Rev. Mol. Cell Biol.* **6,** 476–486
6. Wohlschlegel, J. A., Dhar, S. K., Prokhorova, T. A., Dutta, A., and Walter, J. C. (2002) *Mol. Cell* **9,** 233–240
7. Ricke, R. M., and Bielinsky, A. K. (2004) *Mol. Cell* **16,** 173–185
8. Lee, J. K., Seo, Y. S., and Hurwitz, J. (2003) *Proc. Natl. Acad. Sci. U. S. A.* **100,** 2334–2339
9. Walter, J., and Newport, J. (2000) *Mol. Cell* **5,** 617–627
10. Takayama, Y., Kamimura, Y., Okawa, M., Muramatsu, S., Sugino, A., and Araki, H. (2003) *Genes Dev.* **17,** 1153–1165
11. Pacek, M., and Walter, J. C. (2004) *EMBO J.* **23,** 3667–3676
12. Pacek, M., Tutter, A. V., Kubota, Y., Takisawa, H., and Walter, J. C. (2006) *Mol. Cell* **21,** 581–587
13. Moyer, S. E., Lewis, P. W., and Botchan, M. R. (2006) *Proc. Natl. Acad. Sci.*

U. S. A. **103,** 10236–10241
14. Gambus, A., Jones, R. C., Sanchez-Diaz, A., Kanemaki, M., van Deursen, F., Edmondson, R. D., and Labib, K. (2006) *Nat. Cell Biol.* **8,** 358–366
15. Zegerman, P., and Diffley, J. F. (2007) *Nature* **445,** 281–285
16. Tanaka, S., Umemori, T., Hirai, K., Muramatsu, S., Kamimura, Y., and Araki, H. (2007) *Nature* **445,** 328–332
17. Tanaka, T., and Nasmyth, K. (1998) *EMBO J.* **17,** 5182–5191
18. Zou, L., and Stillman, B. (2000) *Mol. Cell. Biol.* **20,** 3086–3096
19. Yang, X., Gregan, J., Lindner, K., Young, H., and Kearsey, S. E. (2005) *BMC Mol. Biol.* **6,** 13
20. Mimura, S., and Takisawa, H. (1998) *EMBO J.* **17,** 5699–5707
21. Garg, P., and Burgers, P. M. (2005) *Crit. Rev. Biochem. Mol. Biol.* **40,** 115–128
22. Homesley, L., Lei, M., Kawasaki, Y., Sawyer, S., Christensen, T., and Tye, B. K. (2000) *Genes Dev.* **14,** 913–926
23. Izumi, M., Yanagi, K., Mizuno, T., Yokoi, M., Kawasaki, Y., Moon, K. Y., Hurwitz, J., Yatagai, F., and Hanaoka, F. (2000) *Nucleic Acids Res.* **28,** 4769–4777
24. Kawasaki, Y., Hiraga, S., and Sugino, A. (2000) *Genes Cells* **5,** 975–989
25. Christensen, T. W., and Tye, B. K. (2003) *Mol. Biol. Cell* **14,** 2206–2215
26. Gregan, J., Lindner, K., Brimage, L., Franklin, R., Namdar, M., Hart, E. A., Aves, S. J., and Kearsey, S. E. (2003) *Mol. Biol. Cell* **14,** 3876–3887
27. Ricke, R. M., and Bielinsky, A. K. (2006) *J. Biol. Chem.* **281,** 18414–18425
28. Fien, K., Cho, Y. S., Lee, J. K., Raychaudhuri, S., Tappin, I., and Hurwitz, J. (2004) *J. Biol. Chem.* **279,** 16144–16153
29. Fien, K., and Hurwitz, J. (2006) *J. Biol. Chem.* **281,** 22248–22260
30. Das-Bradoo, S., Ricke, R. M., and Bielinsky, A. K. (2006) *Mol. Cell. Biol.* **26,** 4806–4817
31. Cook, C. R., Kung, G., Peterson, F. C., Volkman, B. F., and Lei, M. (2003) *J. Biol. Chem.* **278,** 36051–36058
32. Anumanthan, G., Halder, S. K., Friedman, D. B., and Datta, P. K. (2006) *Cancer Res.* **66,** 10824–10832
33. Philo, J. S. (2000) *Anal. Biochem.* **279,** 151–163
34. Stafford, W. F., 3rd. (1992) *Anal. Biochem.* **203,** 295–301
35. Schuck, P. (2003) *Anal. Biochem.* **320,** 104–124
36. Stafford, W. F., and Sherwood, P. J. (2004) *Biophys. Chem.* **108,** 231–243
37. Laue, T. M., Shah, B., Ridgeway, T. M., and Pelletier, S. L. (1992) *SEDNTERP*, Royal Society of Chemistry, Cambridge, UK
38. Voitenleitner, C., Fanning, E., and Nasheuer, H. P. (1997) *Oncogene* **14,** 1611–1615
39. Smith, D. B., and Johnson, K. S. (1988) *Gene* (*Amst.*) **67,** 31–40
40. Walter, J., Sun, L., and Newport, J. (1998) *Mol. Cell* **1,** 519–529
41. Okorokov, A. L., Waugh, A., Hodgkinson, J., Murthy, A., Hong, H. K., Leo, E., Sherman, M. B., Stoeber, K., Orlova, E. V., and Williams, G. H. (2007) *EMBO Rep.* **8,** 925–930
42. Garcia de la Torre, J. G., and Bloomfield, V. A. (1981) *Q. Rev. Biophys.* **14,** 81–139
43. Kwon, K., Cao, C., and Stivers, J. T. (2003) *J. Biol. Chem.* **278,** 19442–19446
44. Metz, A. H., Hollis, T., and Eichman, B. F. (2007) *EMBO J.* **26,** 2411–2420
45. Michael, W. M., Ott, R., Fanning, E., and Newport, J. (2000) *Science* **289,** 2133–2137
46. Mizuno, T., Yamagishi, K., Miyazawa, H., and Hanaoka, F. (1999) *Mol. Cell. Biol.* **19,** 7886–7896
47. Dornreiter, I., Copeland, W. C., and Wang, T. S. (1993) *Mol. Cell. Biol.* **13,** 809–820
48. Stauffer, M. E., and Chazin, W. J. (2004) *J. Biol. Chem.* **279,** 30915–30918
49. Fanning, E., Klimovich, V., and Nager, A. R. (2006) *Nucleic Acids Res.* **34,** 4126–4137
50. Arunkumar, A. I., Stauffer, M. E., Bochkareva, E., Bochkarev, A., and Chazin, W. J. (2003) *J. Biol. Chem.* **278,** 41077–41082
51. Kelley, L., MacCallum, R., and Sternberg, M. (2000) *J. Mol. Biol.* **299,** 499–520
52. Mer, G., Bochkarev, A., Gupta, R., Bochkareva, E., Frappier, L., Ingles, C. J., Edwards, A. M., and Chazin, W. J. (2000) *Cell* **103,** 449–456
53. Stauffer, M. E., and Chazin, W. J. (2004) *J. Biol. Chem.* **279,** 25638–25645
54. Leon, O., and Roth, M. (2000) *Biol. Res.* **33,** 21–30
55. Klug, A., and Schwabe, J. W. (1995) *FASEB J.* **9,** 597–604
56. Kadrmas, J. L., and Beckerle, M. C. (2004) *Nat. Rev. Mol. Cell Biol.* **5,** 920–931
57. Borden, K. L. (2000) *J. Mol. Biol.* **295,** 1103–1112
58. Murzin, A. G., Brenner, S. E., Hubbard, T., and Chothia, C. (1995) *J. Mol. Biol.* **247,** 536–540
59. Petroski, M. D., and Deshaies, R. J. (2005) *Nat. Rev. Mol. Cell Biol.* **6,** 9–20
60. Zheng, N., Schulman, B. A., Song, L., Miller, J. J., Jeffrey, P. D., Wang, P., Chu, C., Koepp, D. M., Elledge, S. J., Pagano, M., Conaway, R. C., Conaway, J. W., Harper, J. W., and Pavletich, N. P. (2002) *Nature* **416,** 703–709
61. Shamoo, Y., Friedman, A. M., Parsons, M. R., Konigsberg, W. H., and Steitz, T. A. (1995) *Nature* **376,** 362–366
62. Lee, J. Y., Chang, C., Song, H. K., Moon, J., Yang, J. K., Kim, H. K., Kwon, S. T., and Suh, S. W. (2000) *EMBO J.* **19,** 1119–1129
63. Bochkareva, E., Korolev, S., Lees-Miller, S. P., and Bochkarev, A. (2002) *EMBO J.* **21,** 1855–1863
64. Jiang, X., Klimovich, V., Arunkumar, A. I., Hysinger, E. B., Wang, Y., Ott, R. D., Guler, G. D., Weiner, B., Chazin, W. J., and Fanning, E. (2006) *EMBO J.* **25,** 5516–5526
65. Collins, K. L., Russo, A. A., Tseng, B. Y., and Kelly, T. J. (1993) *EMBO J.* **12,** 4555–4566
66. Ott, R. D., Rehfuess, C., Podust, V. N., Clark, J. E., and Fanning, E. (2002) *Mol. Cell. Biol.* **22,** 5669–5678